ISSN1027-5495. Functional Materials, 32, No.1 (2025), p. 134-145
doi:http://dx.doi.org/10.15407/fm32.01.134

Comparative qualitative analysis of hot pressing of zirconium dioxide nanopowders

***E.S.Hevorkian*[1], *M.Rucki*[2], *R.V.Vovk*[3], *V.P.Nerubatskyi*[4], *D.Pieniak*[5], *V.O.Chyshkala*[3]**

[1]University of Life Sciences in Lublin, 13 Akademicka, 20-950 Lublin, Poland
[2]Casimir Pulaski Radom University, 54 Stasieckiego Sq.,
26-600 Radom, Poland
[3]V.N.Karazin Kharkiv National University, 4 Svobody Sq.,
61022 Kharkiv, Ukraine
[4]Ukrainian State University of Railway Transport, 7 Feierbakh Sq.,
61050 Kharkiv, Ukraine
[5] Faculty of Safety Engineering and Civil Protection, Fire University, 52/54
Słowackiego Street, 01-629 Warsaw, Poland

Received October 21, 2024

The presented study confirms that the reduction of the level of structural dimensions to the submicron and nanometric ranges is the dominant trend in the development of structural and instrumental ceramics. Following this trend with the use of traditional methods leads to an increase in cost and a significant growth of grains, which requires the introduction of additional preliminary operations, such as grinding of grains and selection of starting powders. At the same time, the application of the method of electroconsolidation under pressure in a vacuum promotes the acceleration of compaction processes, which makes it possible to overcome the shortcomings of traditional approaches when obtaining fine-dispersed, high-density ceramic structures.

Keywords: amorphization, composite, electroconsolidation, sintering, zirconium dioxide.

Порівняльний якісний аналіз гарячого пресування нанопорошків діоксиду цирконію. *Е.С.Геворкян, M.Rucki, Р.В.Вовк, В.П.Нерубацький, D.Pionak, В.О.Чишкала*

Представлене дослідження підтверджує, що зниження рівня структурної розмірності до субмікронного та нанометричного діапазонів є домінуючою тенденцією у розвитку конструкційної та інструментальної кераміки. Дотримання цієї тенденції з використанням традиційних методів призводить до збільшення собівартості та значного зростання зерен, що вимагає впровадження додаткових попередніх операцій, таких як розмелювання зерен та селекція вихідних порошків. У той же час застосування методу електроконсолідації під тиском у вакуумі сприяє прискоренню процесів ущільнення, що дає змогу подолати недоліки традиційних підходів при отриманні тонкодисперсних високощільних керамічних структур.

1. Introduction

The structure and performance properties of ceramic materials obtained using powder technologies are largely determined by the characteristics of the starting powders. The use of nanosized powders creates opportunities for the development of high-density ceramic materials with increased dispersion, and also opens up new prospects for improving their functional characteristics.

To achieve high uniformity of the ceramic structure and reliable manifestation of the expected properties, it is necessary to work with powders of a high degree of homogeneity, the size of individual grains of which is in the range of several tens of nanometers [1, 2].

Qualitative and quantitative analysis of the morphology, dispersion, and phase composition of powders is the basis of modern approaches to predicting the behavior of ceramic products in operation at the preparatory stage of their production. This analysis makes it possible to make the necessary adjustments to the initial powder composition and make reasonable structural and parametric decisions within the framework of the selected system of controlling influences during sintering. Considering the increased polyvariance of modes, which is characteristic of the implementation of combined technological methods, including SPS (Spark Plasma Sintering) technologies [3] and the method of electroconsolidation under pressure [4], developed and applied in the author's experience, this approach significantly improves the quality of final products [5].

An obvious difficulty in obtaining materials with a homogeneous structure based on nanopowder technologies is the tendency of nanosized powders to agglomerate [6]. The manifestation of a tendency to agglomerate and the heterogeneity of the granulometric composition of the initial filling of nanopowders leads to increased heterogeneity of sintered structures, the manifestation of which is their porosity and low density, which leads to reduced strength of ceramic products and incomplete realization of the potential of the nanocrystalline powder base in them [7].

Supplementing sintering with mechanical pressure has a twofold effect on the reformation of the structure of agglomerated ultrafine powders. On the one hand, against the background of the destruction of mainly large structural elements of the powder, its additional activation occurs: the formation of new surfaces, cleaning of boundaries from adsorbed gases. On the other hand, the aggregation of mainly small structural elements of the powder and, accordingly, the reverse effects occur. If it is possible to maintain a balanced manifestation of both opposing trends, then the homogeneity of the sintered sample improves, but still with a loss of the original, non-agglomerated dimensionality of the structural elements of the powder.

The study of particle morphology after preliminary mechanical processing of nanopowders in a drum mill shows [8] that with increasing processing time, firstly, there comes a point when its further continuation does not lead to a noticeable decrease in the average size of individual particles, which is also confirmed by the stabilization of the specific surface area (surface area of grains constituting a weight unit), which is determined by the BET method (Brunauer-Emmett-Teller method) [9]; secondly, the powder compaction (bulk density) continuously increases with a gradual decrease in the growth intensity.

Due to the complex effect on the structure, in which additional "activation" of the powder can be observed due to an increase in the defectivity of the crystal lattice, consolidation under pressure is recognized as a promising resource for reducing the sintering temperature of nanocrystalline powders [10]. At the same time, the study of the influence of high pressures (up to 1 GPa and above) on the structure and phase composition of nanocrystalline powders from the standpoint of expanding the possibilities of forming given structures is highlighted as an independent task [11, 12].

Zirconium dioxide-based materials are very promising for use in various industries: they are widely used in the production of refractory products, high-temperature heaters, heat-resistant enamels, refractory glass, various types of ceramics, ceramic pigments, solid electrolytes, thermal protective coatings, etc. [13, 14].

Undoubtedly, zirconium oxide has sufficiently high mechanical properties for use as both an instrumental and structural material [15–17]. The mechanism of transformation strengthening during the transition from the tetragonal to the monoclinic phase has been studied in considerable detail in many publications [18, 19].

In our opinion, transformation processes affect not only the microstructure and morphology due to distortion of the crystal lattice, but also the bond strength at grain boundaries. From this point of view, the processes occurring during the sintering of partially stabilized zirconia nanopowders by the electroconsolidation method (electrosintering) are extremely interesting, since the electric current affects the surface layers of nanograins [20, 21]. The spark formed between the grains cleans the contact surfaces of the grains, thereby strengthening the bond between the grains [22–24].

In addition, the high heating rate prevents rapid grain growth. At the same time, the shrinkage process proceeds very intensively,

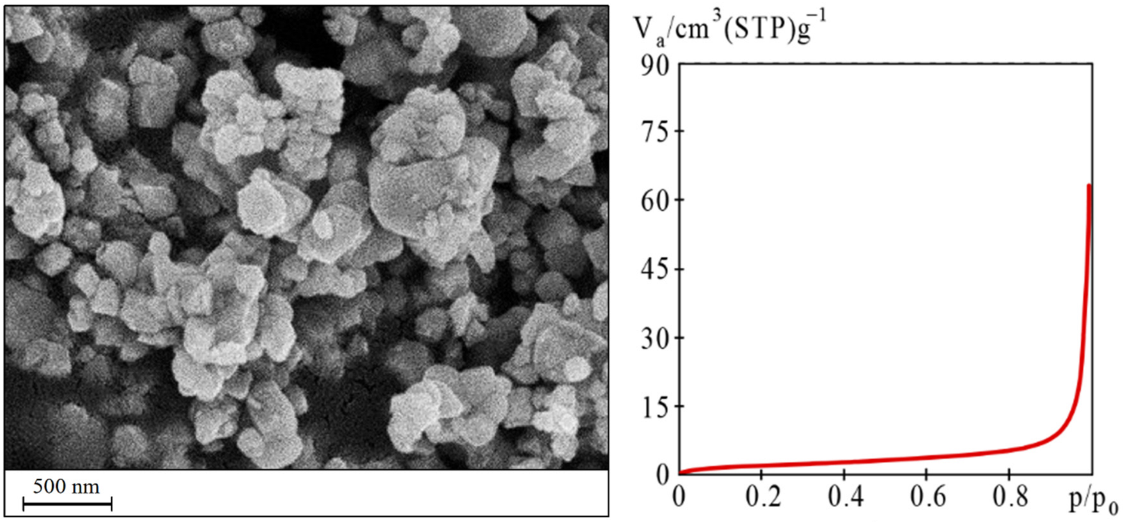

a) b)

Fig. 1. Appearance (a) and characteristics (b) of ZrO_2–3mol.%Y_2O_3 nanopowders determined by the BET method

which allows for rapid densification of the nanopowder mixture. Sintering mechanisms quickly alternate with each other, giving a cumulative effect on the formation of the microstructure of the sintered material.

The purpose of this study is to determine the optimal sintering temperature of zirconium dioxide nanopowders partially stabilized by yttrium oxide with additives of silicon carbide nanopowders, at which the highest density and mechanical properties of the obtained samples are ensured, as well as to assess the homogeneity of the structure and identify the features of the formation of the microstructure and phase composition of the material during rapid heating during electroconsolidation.

2. Materials and methods

The studies used ZrO_2–3mol.%Y_2O_3 nanopowders (Zhengzhou Xinli Wear-Resistant Material Co., Ltd.), manufactured in Henan (China).

The used ZrO_2–3mol.%Y_2O_3 nanopowder (Fig. 1) had a specific surface area of 9.4 m^2/g, ZrO_2 – 94.4 wt.%, Y_2O_3 – 5.25±0.25 wt.%, SiO_2 – 0.0092 wt.%, Fe_2O_3 – 0.0014 wt.%, TiO_2 – 0.0009 wt.%.

Fig. 2 shows silicon carbide (SiC) nanopowders manufactured by Nanostructured & Amorphous Materials (USA).

Sintering of nanopowders was carried out by the electroconsolidation method on a developed, manufactured, and hinged author's installation, the principle of operation of which was considered [25].

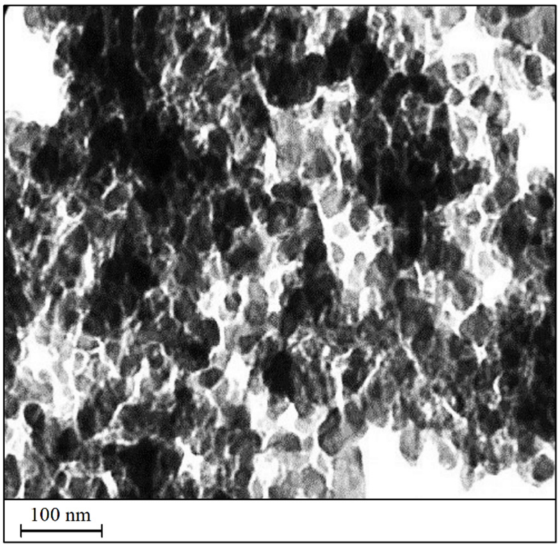

Fig. 2. SiC nanopowders

To determine the specific surface area of nanopowders, the BET method was used, which is used in devices such as BELSORP-mini II (BEL JAPAN, INC). This method is used to determine the specific surface area of a material, especially porous substances.

For X-ray diffraction studies, X-ray diffraction measurements were executed by XRD diffractometer MiniFlex600 (RIGAKU, Japan) using Co Kα radiation (λ = 0.179 nm) with the voltage and emission current set to be 40 kV and 15 mA, respectively. Diffraction patterns were recorded in the diffraction angle 2θ ranging from 3 to 90° at the scanning speed of 10°/min and step 0.2°.

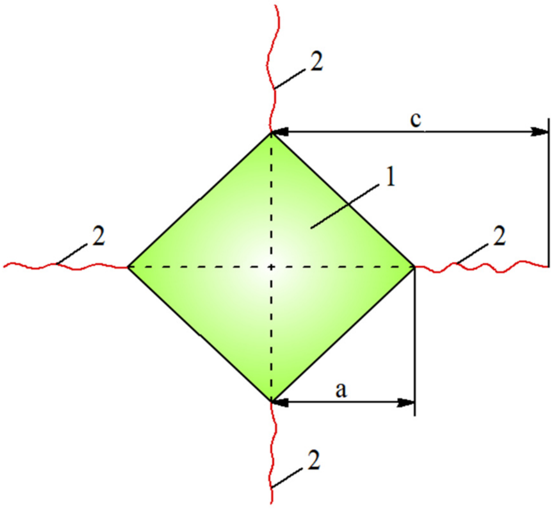

Fig. 3. Illustration of a Vickers indenter impression (1) with radial cracks (2)

The surface of the samples was studied using a Hitachi SU-70 field emission scanning electron microscope equipped with an electron gun with a Schottky thermal emitter. A Thermo Scientific EDS-type X-ray microanalyzer was used, which allows the detection of elements from beryllium to uranium with the acquisition of an X-ray spectrum depending on the radiation energy characteristic of a given element (qualitative and quantitative analysis).

Crack resistance was determined using a diamond pyramid indenter. If crack propagation occurs from the corners of the Vickers indenter impression, the stress intensity coefficient (K_{IC}) of the material can be determined. This is the so-called first case of Griffiths cracking – a crack in a specific loading case. To determine the K_{IC}, the crack length c and the diagonal indentations a were measured (Fig. 3).

Then, the crack resistance can be calculated using the expression:

$$K_{IC} = 0{,}067 \cdot \left(\frac{E}{HV}\right)^{0{,}4} \cdot \left(\frac{c}{a}\right)^{-1{,}5} \cdot HV \cdot \sqrt{a}, \quad (1)$$

where a is half of the diagonal of the imprint [m]; HV is the hardness [GPa]; E is the modulus of elasticity [GPa]; c is the crack length [m].

Nanoindentation was carried on an Agilent/Keysight G200 Nanoindenter using a diamond Berkovich tip. Continuous stiffness measurement (CSM) mode was applied in displacement-controlled mode (via a force feedback loop) with a maximum penetration depth of 300 nm and a constant strain rate of 0.05 s^{-1}. Indentation was performed on both the polished, non-deformed sample surface and in an appropriate part of the wear tracks. Indents were arranged in grids of 8×8 and 5×5, respectively for the non-deformed surface and wear tracks, with a distance between the indents of 6 μm, which is sufficiently large to avoid the interaction of stress fields of adjacent indents.

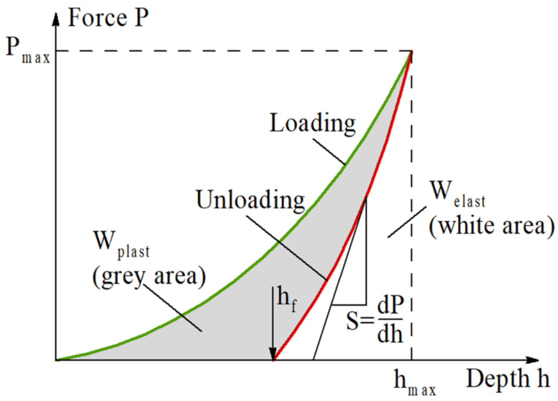

Fig. 4. Theoretical characteristics of the displacement force with an indication of important parameters of the indentation test during nanoindentation

During the nanoindentation process, surface mapping was performed, i.e., the hardness distribution of the sample surface zones was determined (Fig. 4).

The samples under study contain agglomerates, which are not entirely homogeneous materials. The test was aimed at evaluating the mechanical properties of the matrix and dispersed grains (inclusions). The Hysitron TS77 Select device was used to evaluate the mechanical properties of the material phases. The In-Situ SPM Imaging method was used. In this method, a topographic survey of the surface is performed using an indenter (a Berkovich indenter was used, the projected contact area $A = 24{,}5hc^2$), and nanomechanical properties are simultaneously determined. Mapping was performed and the hardness was determined according to the equation [26]:

$$H_{IT} = \frac{P_{max}}{A}, \quad (2)$$

where the indentation hardness H_{IT} was determined by the ratio of the largest normal force P_{max} loading the indenter to the indenter contact area at maximum load A.

3. Result and discussion

It is known [27] that technical ceramics made from powders based on zirconium dioxide partially stabilized with yttrium oxide have

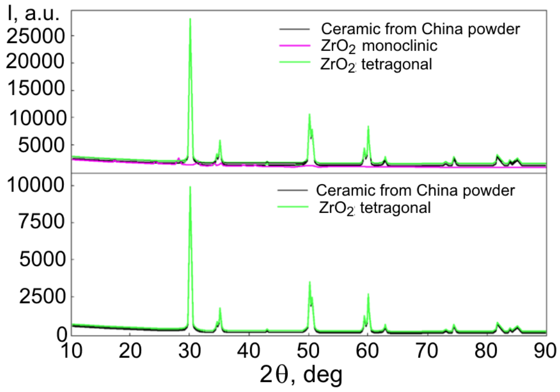

Fig. 5. X-ray phase analysis of the initial ZrO_2–3mol.%Y_2O_3 nanopowder and sintered by the electroconsolidation method at a temperature of 1400°C

a unique set of physical and mechanical properties: high strength, hardness and fracture toughness, resistance to corrosion and wear. Studies of sintering processes by the electroconsolidation method were carried out with both partially stabilized zirconium dioxide and mixtures of zirconium oxide, silicon carbide, and tungsten monocarbide. It is obvious that refractory carbides have high hardness and their addition to zirconium oxide provides the necessary properties for using the composite as an instrument [28–30].

As shown by X-ray phase analysis of the starting powder partially stabilized with yttrium oxide nanopowder, the tetragonal phase predominates in it (Fig. 5).

Applying pressures from 1 to 9 GPa to consolidated ceramic nanopowders [31, 32] makes it possible to overcome interparticle friction and break down agglomerates to obtain high-density crystalline samples with a nanograin structure. However, the implementation of such pressures poses certain technological difficulties.

Usually, often in practice, a three-stage process is used to obtain ceramic nanomaterials with high mechanical characteristics: preliminary pressing of powders in a normal atmosphere, subsequent sintering of prepared compacts in an air environment at temperatures above 1000°C, and final hot isostatic pressing [33]. For example, in obtaining ZrO_2 products according to this scheme, the duration of the thermally loaded second and third stages can be from 2 to 6 hours and from 2 to 3 hours at temperatures from 1100 to 1300°C and from 1150 to 1350°C, respectively [34].

The development and expanded reproduction of more technologically advanced and less energy-intensive sintering processes for nanocrystalline materials is a scientific and industrial priority.

Reducing the sintering temperature of nanocrystalline samples, in addition to directly reducing the cycle time of manufacturing ceramic products, also has an indirect effect on it with the same trend.

Studies [35] have shown that by changing the heating rate, it is possible to purposefully vary the shrinkage (densification) of the nanocrystalline powder system at the isothermal holding stage; at the same time, lower sintering temperatures correspond to faster densification at the isothermal stage. It is also noted there that the formation of highly dispersed oxide structures under the influence of mechanical processing of partially aggregated nanosized powders is accompanied by a kind of “halo” around the particles recorded in SEM images, which may be evidence of amorphization of the powder during mechanical impact.

In pressure electroconsolidation technologies [36, 37], the intensity and nature of the direct mechanical impact on the powder system, carried out in a mold with a uniaxial load, are inclined towards lower tension, differing from shock wave treatment according to the method [38] or improving the morphology of particles pre-treated in a mechanical mill, which, according to observations, leads to partial amorphization of the powder. However, the shock-wave effects of spark discharges in a powder medium consolidated under direct electric heating with alternating electric current [39] lead to the formation and maintenance of amorphized near-surface “white” layers, which can be considered as possible provocateurs of partial amorphization, for example, oxide products of the highly quasi-explosive [40] shock compression mechanism in the spot of the spark discharge channel.

When determining the modes of electroconsolidation under pressure of zirconium dioxide stabilized, for example, by yttrium [41, 42], special attention should be paid to preventing conflicts with operational parameters [43] and the phenomena of mass transformation of the tetragonal T-phase into the monoclinic M-phase, due to the possible shock-wave consequences of spark discharges. Grain growth using fine-crystalline powders compared to coarse-crystalline powders, when the level of stored deformation energy, which finds an outlet in the transformation T→M transition, can increase signifi-

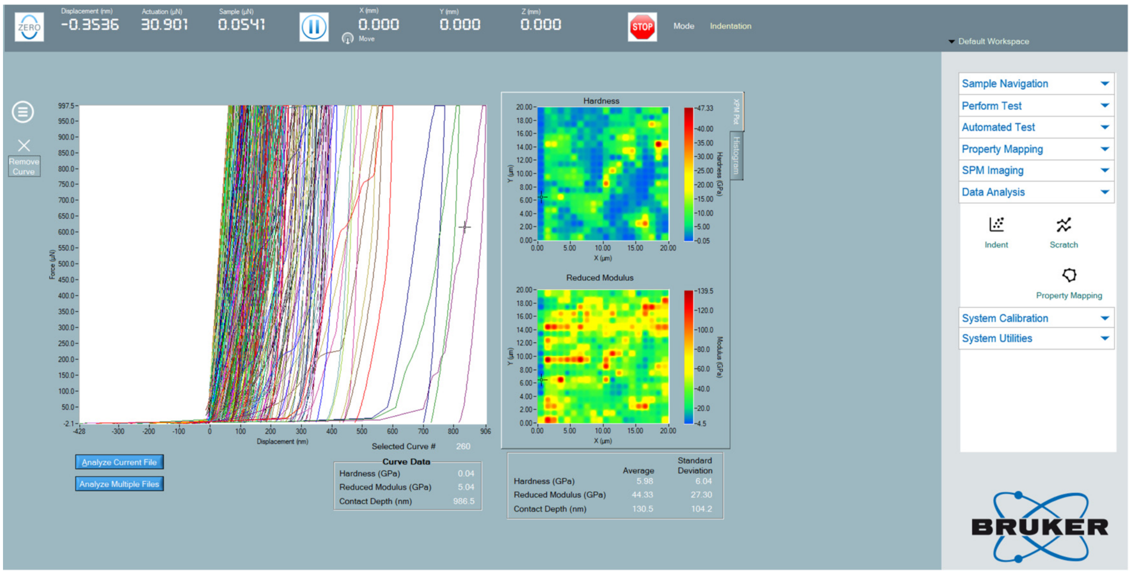

Selected Curve # 260

Curve Data	
Hardness (GPa)	0.04
Reduced Modulus (GPa)	5.04
Contact Depth (nm)	986.5

	Average	Standard Deviation
Hardness (GPa)	5.98	6.04
Reduced Modulus (GPa)	44.33	27.30
Contact Depth (nm)	130.5	104.2

Fig. 6. Distribution of nanohardness and elastic modulus for samples obtained by the method of electroconsolidation of the ZrO_2–3mol.%Y_2O_3 mixture at a sintering temperature of 1200ºC, a holding time of 2 minutes and a pressure of 45 MPa

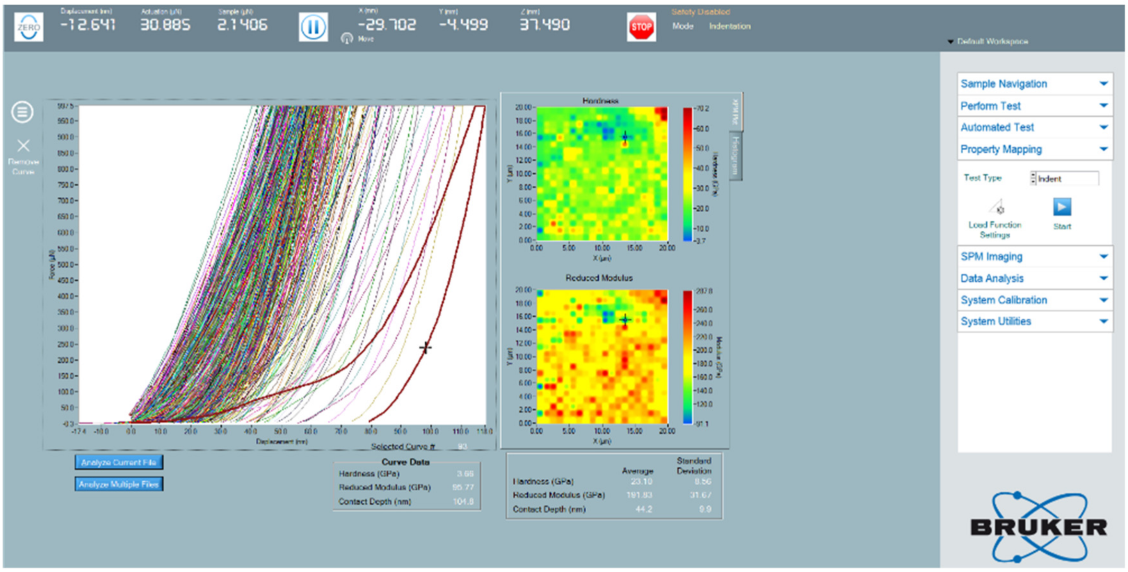

Selected Curve # 93

Curve Data	
Hardness (GPa)	3.66
Reduced Modulus (GPa)	95.77
Contact Depth (nm)	101.8

	Average	Standard Deviation
Hardness (GPa)	23.10	8.56
Reduced Modulus (GPa)	191.83	31.67
Contact Depth (nm)	44.2	9.9

Fig. 7. Distribution of nanohardness and elastic modulus for samples obtained by the method of electroconsolidation of the ZrO_2–3mol.%Y_2O_3–10wt.%SiC mixture at a sintering temperature of 1400ºC, a holding time of 2 minutes and a pressure of 45 MPa

cantly (several times). At the same time, for specific conditions (impact load pressure) there is a critical particle size d_k, exceeding which crystallites must transform into an operationally undesirable M-phase of reduced strength [44]. According to the data, which converge in the order of the obtained results [45], $d_k \approx 10$ nm and less corresponds to the impact load pressure within 20…30 GPa. Below, Fig. 6, 7, 8 show how the nanohardness and elastic modulus of samples sintered under different regimes change.

From Fig. 8 it can be seen that with increasing temperature not only does the hardness increase, but also the heterogeneity of the composite decreases.

Fig. 9 shows the distribution of nanohardness values over the surface of the studied sintered sample ZrO_2–3mol.%Y_2O_3–10wt.%SiC.

Fig. 10 shows that the nanohardness distribution is significantly affected by the sintering time. Increasing the isothermal holding time to 10 min reduces the spread of nanohardness values compared to a sintering time of 2 min, which indicates higher material homogeneity.

Fig. 11 shows an increase in nanohardness values on the sample surface with increasing sintering time up to 10 minutes.

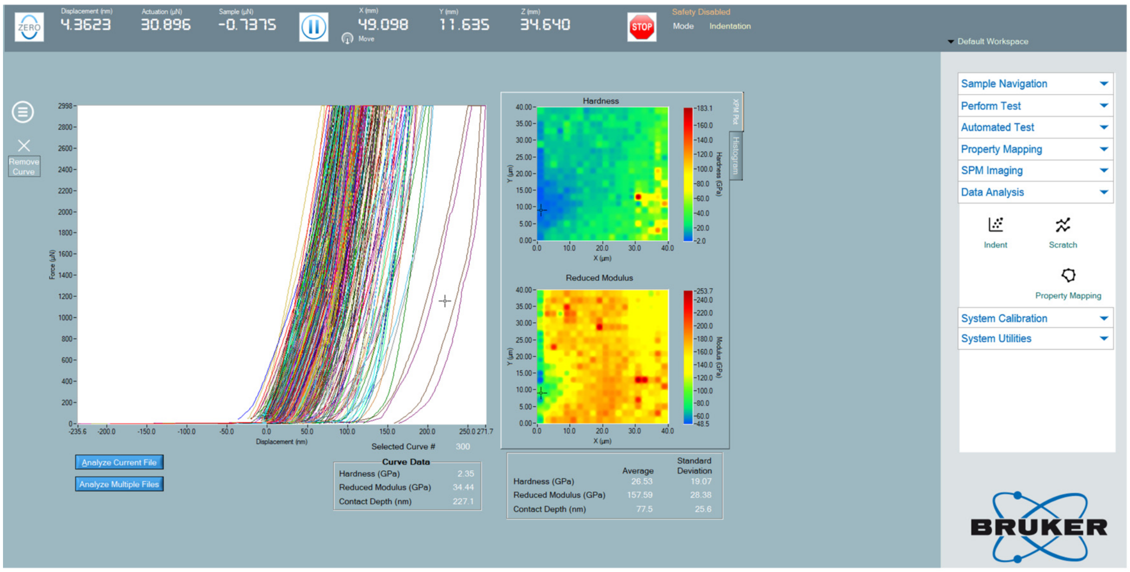

Displacement (nm) 4.3623
Actuation (µN) 30.896
Sample (µN) -0.7375
X (mm) 49.098
Y (mm) 11.635
Z (mm) 34.640
Mode Indentation

Selected Curve # 300

Curve Data	
Hardness (GPa)	2.35
Reduced Modulus (GPa)	34.44
Contact Depth (nm)	227.1

	Average	Standard Deviation
Hardness (GPa)	26.53	19.07
Reduced Modulus (GPa)	157.59	28.38
Contact Depth (nm)	77.5	25.6

Fig. 8. Distribution of nanohardness and elastic modulus for samples obtained by the method of electroconsolidation of the ZrO_2–3mol.%Y_2O_3–10wt.%SiC mixture at a sintering temperature of 1600ºC, a holding time of 2 minutes and a pressure of 45 MPa

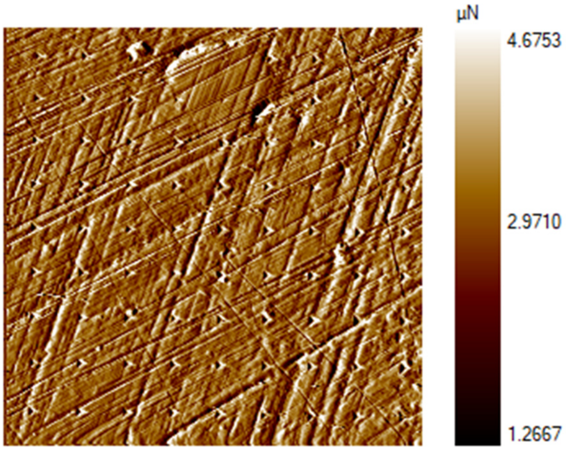

Fig. 9. Distribution of nanohardness values over the surface of the studied sintered sample ZrO_2–3mol.%Y_2O_3–10wt.%SiC at a sintering temperature of 1400ºC, a holding time of 2 minutes and a pressure of 45 MPa

During the electroconsolidation process, there may be an increase in microdistortions of the crystal lattice of the tetragonal T-phase as a result of the formation of a solid solution of $(Zr_{0.6}Y_{0.4})O_{1.8}$, which leads to its destabilization and transformation into a monoclinic modification, and an increase in residual temperatures leads to the relaxation of the deformation energy and the complete disappearance of the M-phase. The X-ray diffraction pattern (Fig. 12) shows the formation of a solid solution and the absence of a monoclinic phase.

This dimensional characteristic of the powder corresponds to a certain critical value of the impact pressure (compression) P_k, at which in a certain region $P_k+\Delta P_k$, as a rule, heating to high residual temperatures of recrystallization annealing is preceded. It is obvious that this reduces the level of crystallographic microdistortions and, accordingly, the formation of the monoclinic M-phase. Thus, all particles undergo a T→M phase transformation. It should be assumed that the magnitude of the lattice mi-

Table 1. Distribution of chemical elements of the sample (isothermal exposure 2 minutes)

Spectrum	In stats.	C	N	O	Si	Y	Zr	Total
Spectrum 1	Yes	61.71	12.32	12.89	2.49	1.16	9.43	100.00
Spectrum 2	Yes	64.10	14.04	19.91	1.95	0.00	0.00	100.00
Spectrum 3	Yes	33.15	–	13.90	5.56	5.26	42.12	100.00
Spectrum 4	Yes	31.67	–	16.67	4.36	4.01	43.28	100.00
Spectrum 5	Yes	33.73	–	10.11	9.62	5.18	41.36	100.00
Spectrum 6	Yes	33.69	–	10.46	9.77	3.17	42.90	100.00
Spectrum 7	Yes	37.62	–	11.97	10.79	4.16	35.47	100.00
Max.	–	64.10	14.04	19.91	10.79	5.26	43.28	–
Min.	–	31.67	12.32	10.11	1.95	0.00	0.00	–

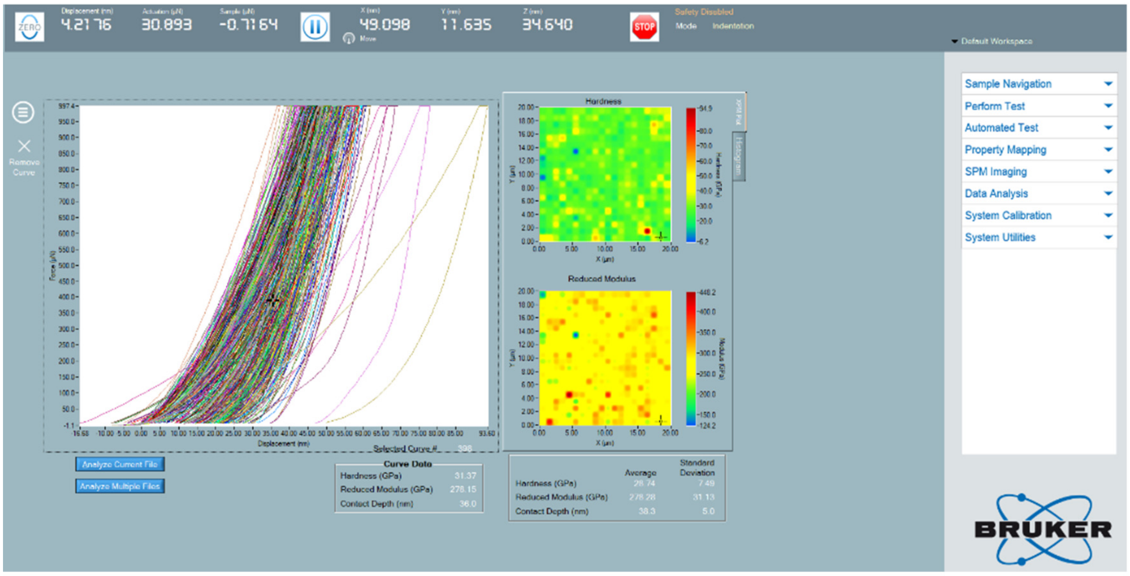

Curve Data

Hardness (GPa)	31.37
Reduced Modulus (GPa)	278.15
Contact Depth (nm)	36.0

	Average	Standard Deviation
Hardness (GPa)	28.74	7.49
Reduced Modulus (GPa)	278.28	31.13
Contact Depth (nm)	38.3	5.0

Fig. 10. Distribution of nanohardness and elastic modulus for samples obtained by the method of electroconsolidation of the ZrO_2–3mol.%Y_2O_3–10wt.%SiC mixture at a sintering temperature of 1600°C, a holding time of 10 minutes and a pressure of 45 MPa

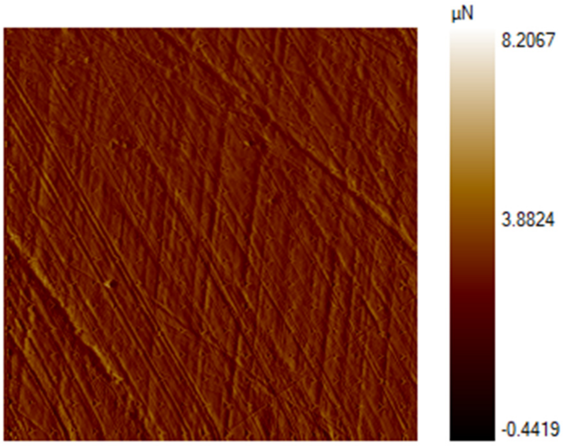

Fig. 11. Distribution of nanohardness values over the surface of the studied sintered sample ZrO_2–3mol.%Y_2O_3–10wt.%SiC at a sintering temperature of 1400°C, a holding time of 10 minutes and a pressure of 45 MPa

crodistortions increases with a decrease in its average bulk crystal size d, which follows from the hypothetical feature of microdistortions at the phase interface.

A similar picture should obviously be expected in electrosintering technologies for some small value of d in a certain system of volt-ampere and frequency characteristics of the current supply to the sintering object: the higher the power of the current supply, the greater the value of microdistortions of the crystal lattice. The subjection of a particle to electric discharge surface effects can essentially be considered as a bulk phenomenon with a predominant effect on the particle as a whole, and not only on the state of its surface layer.

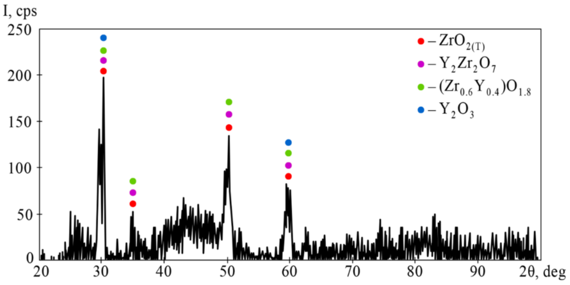

Fig. 12. X-ray diffraction pattern of a ZrO_2–3mol.%Y_2O_3 sample sintered at a temperature of 1200°C and an isothermal holding time of 10 minutes

The formation of microdistortions in the crystal lattice affects the microstructure and properties not only for ZrO_2, but also for ZrO_2–3mol.%Y_2O_3–10wt.%SiC composites. Microanalysis at different points on the composite surface is presented in Fig. 13. The chemical composition at different points is given in Table 1. Increasing the sintering time at a temperature of 1600°C from 2 minutes to 10 minutes leads to a significant change in the chemical composition, shown in Fig. 14.

Chemical analysis of the composition at different points of the sample is given in Table 2.

Since the fracture in pressed partially stabilized zirconia is caused by the tetragonal-monoclinic T→M phase transformation, when the volume growth in their cells corresponding to these transformations, known [41], leads to cracking of individual particles and the sintered material as a whole, it is possible to determine the value of the pressing pressure at which the destruction of the structural elements of the

Table 2. Distribution of chemical elements of the sample (isothermal exposure 10 minutes)

Spectrum	In stats.	C	O	Si	Y	Zr
Spectrum 1	Yes	74.06	14.90	0.92	1.01	9.10
Spectrum 2	Yes	78.48	7.10	12.30	0.00	2.12
Spectrum 3	Yes	64.08	23.63	1.16	1.28	9.85
Spectrum 4	Yes	69.22	14.76	13.52	0.24	2.26
Spectrum 5	Yes	75.95	5.73	15.80	0.33	2.19
Mean	–	72.36	13.22	8.74	0.57	5.10
Std. deviation	–	5.74	7.20	7.14	0.55	4.00
Max.	–	78.48	23.63	15.80	1.28	9.85
Min.	–	64.08	5.73	0.92	0.00	2.12

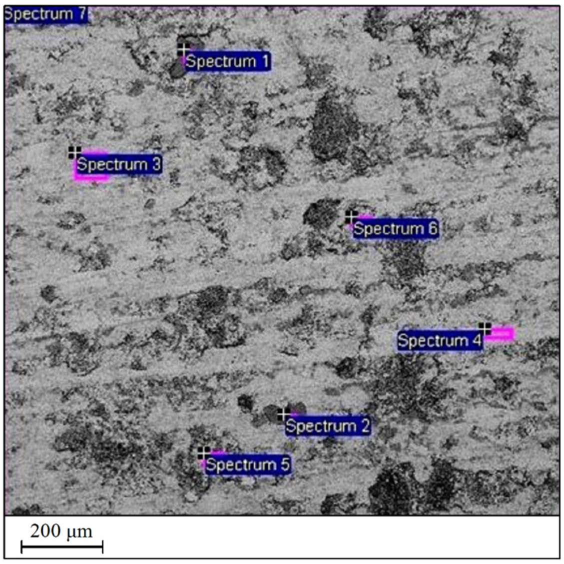

Fig. 13. Sintered sample ZrO_2–3mol.%Y_2O_3–10wt.%SiC at a temperature of 1600ºC, isothermal holding time of 2 minutes and pressure of 45 MPa

powder begins, based on the increase in the monoclinic M phase in the pressings relative to its amount in the initial powder.

Taking this into account, as well as with an adjustment for the possible provocation of intensification of the T→M phase transition in the zones of action of spark discharges during electrosintering, which is practiced in the entire nanoscale range $d < 100$ nm, including at $d > 40$ nm, it is possible to recommend for preliminary experiments with sintering ZrO_2–3mol.%Y_2O_3 a uniaxial load of no higher than 30...40 MPa.

The kinetics of rapid shrinkage in the compaction of nanocrystalline powders at the non-isothermal stage of sintering is determined by the mechanisms of substance transfer by mutual slipping of powder particles, and at the initial stage of sintering, which is especially active due to the relatively high porosity, as well as by compaction due to recrystallization grain growth.

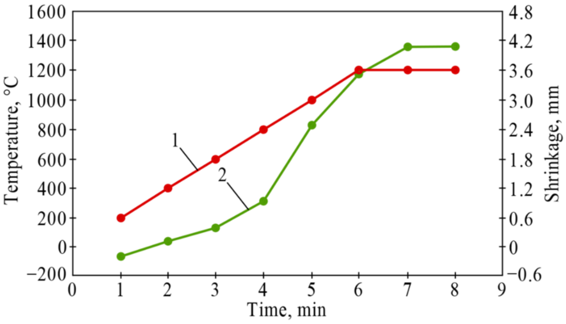

Fig. 14. Sintered sample ZrO_2–3mol.%Y_2O_3–10wt.%SiC at a temperature of 1600ºC, isothermal holding for 10 minutes and a pressure of 45 MPa

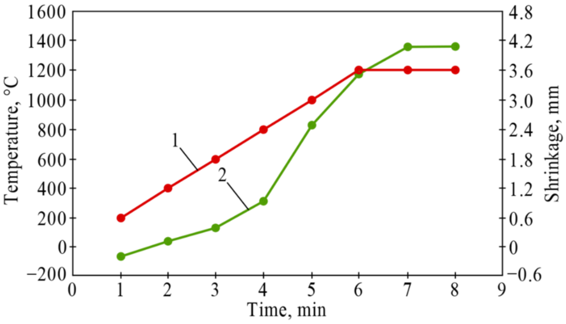

Fig. 15. Dependence of temperature (1) and shrinkage (2) on heating time

It should be assumed that, perhaps, in the isothermal stage of sintering, the established thermodynamic equilibrium inhibits the active displacement of particles. By setting the value of the function in the equation of shrinkage kinetics to zero ($\Delta L/L = k\cdot\tau^n$, where $\Delta L/L$ is the relative shrinkage, k is the kinetic coefficient of the process rate, n is a constant reflecting the densification mechanism; according to the data under conditions of $n = 0.02$) and solving the inverse problem $n = f(\Delta L/L)$, we can proceed to determine the heating temperature to the isothermal holding, at which the densification of ceramics will not occur (Fig. 15).

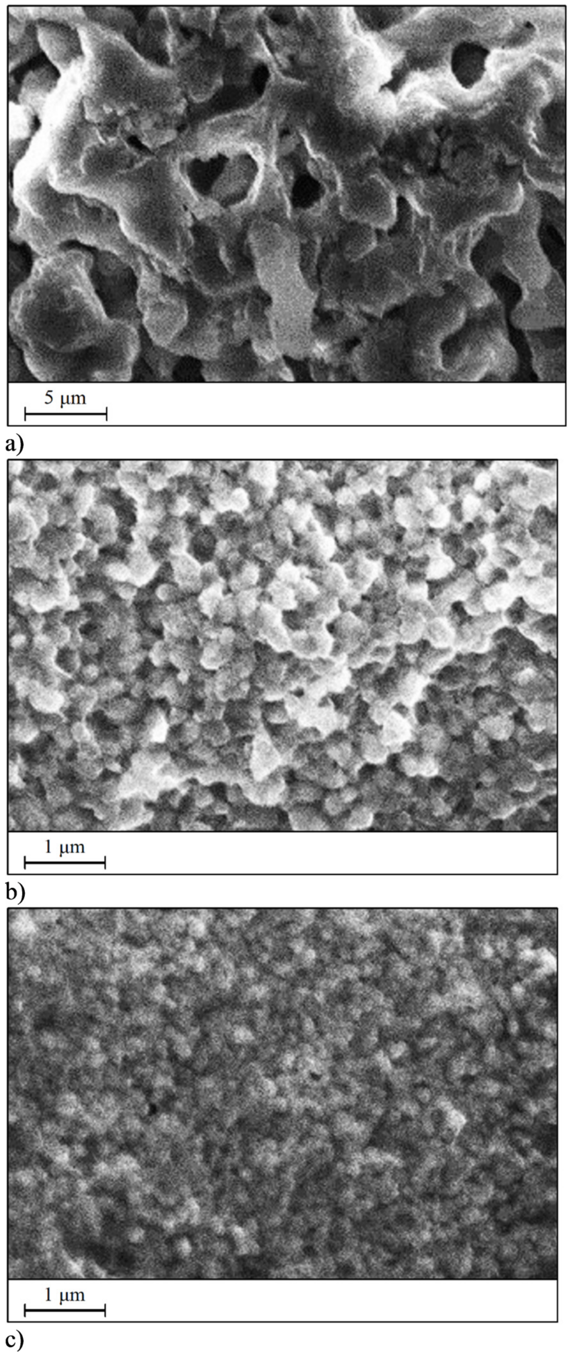

Fig. 16. Microstructure of the ZrO_2–3mol.%Y_2O_3 material sintered by the electroconsolidation method under the following conditions: temperature 1400°C, holding time 10 minutes, pressure 45 MPa (a); temperature 1400°C, holding time 3 minutes, pressure 45 MPa (b); temperature 1500°C, holding time 3 minutes, pressure 45 MPa (c)

In our experiments, the best result, combining high density, dispersion, relative uniformity of grain distribution and, obviously, due to the above, the most viscous nature of fracture, corresponds to a grain structure within 250...300 nm, obtained by implementing an electric heating cycle with a final isothermal holding temperature of 1400°C when using a ZrO_2–3mol.%Y_2O_3 nanopowder from spherical particles with initial average sizes mainly within 20...30 nm (Fig. 16). The crack resistance of this sample was 12...14 MPa·$m^{1/2}$.

For comparison, nanocrystalline powders specially prepared for subsequent sintering by pre-pressing (pressure 10 MPa) in experimental practice have an initial size distribution within the range of up to 50 nm, with at least 95% of grains not exceeding 40 nm, and their average size is in the range of 20…30 nm.

It should be noted that the studied electroconsolidation process is significantly more efficient in terms of energy consumption than other SPS methods, given that its optimal temperature peak (0.36 in the dimensionless homologous estimate) does not exceed 65% of the values in the recommended [44] temperature range (0.56…0.63).

4. Conclusion

Thus, accelerated heating of a nanopowder mixture during sintering by the electroconsolidation method, carried out in combination with uniaxial compression, can be considered a reliable thermomechanical basis for the production of high-density, highly functional and competitive submicro- and nanoceramics. This is especially true for the products of the tool industry, the quality of which significantly affects the technical and economic success of mechanical processing enterprises in various industries. In this regard, the presented electroconsolidation technology is an important resource for the progressive development and continuity of technological systems.

Acknowledgments

This study was supported through project MSCA4Ukraine financed by the European Union.

References

1. A.Goldstein, N.Travitzky, A.Singurindy, M.Kravchik, *Journal of the European Ceramic Society*, **19(12)**, 2067–2072 (1999). doi: https://doi.org/10.1016/S0955-2219(99)00020-5.
2. G.D.Quinn, J.Eichler, U.Eisele, J.Rodel, *Journal of the American Ceramic Society*, **87(3)**, 513–516 (2004). doi: https://doi.org/10.1111/j.1551-2916.2004.00513.x.

3. Z.Shen, L.Liu, X.Xu, J.Zhao, M.Eriksson, Y.Zhong, E.Adolfsson, Y.Liu, A.Kocjan, *Journal of the European Ceramic Society*, **37(14)**, 4339–4345 (2017). doi: https://doi.org/10.1016/j.jeurceramsoc.2017.03.008.
4. E.S.Hevorkian, V.P.Nerubatskyi, M.Rucki, A.Kilikevicius, A.G.Mamalis, W.Samociuk, D.Morozow, *Nanotechnology Perceptions*, **20(1)**, **100**–113 (2024**).** doi: https://doi.org/10.56801/nano-ntp.v20i1.363.
5. T.Zhu, Z.Xie, *Journal of the American Ceramic Society*, **105(3)**, 1617–1621 (2022). doi: https://doi.org/10.1111/jace.18178.
6. W.H.Rhodes, *Journal of the American Ceramic Society*, **64(1)**, 19–22 (1981). doi: https://doi.org/10.1111/j.1151-2916.1981.tb09552.x.
7. N.Bamba, Y.H.Choa, T.Sekino, K.Niihara, *Journal of the European Ceramic Society*, **23(5)**, 773–780 (2003). doi: https://doi.org/10.1016/S0955-2219(02)00168-1.
8. M.S.El-Eskandarany, A.Al-Hazza, L.A.Al-Hajji, N.Ali, A.A.Al-Duweesh, M.Banyan, F.Al-Ajmi, *Nanomaterials*, **11(10)**, 2484 (2021). doi: https://doi.org/10.3390/nano11102484.
9. P.Sinha, A.N.Datar, C.Jeong, X.Deng, Y.G.Chung, L.-C.Lin, *The Journal of Physical Chemistry C*, **123(33)**, 20195–20209 (2019). doi: https://doi.org/10.1021/acs.jpcc.9b02116.
10. M.I.Kabanova, V.A.Dubok, S.A.Nochevkin, *Poroshkovaya metallurgiya*, **9**, 69–74 (1991) (in Russian).
11. J.Chevalier, L.Gremillard, A.V.Virkar, D.R.Clarke, *Journal of the American Ceramic Society*, **92(9)**, 1901–1920 (2009). doi: https://doi.org/10.1111/j.1551-2916.2009.03278.x.
12. K.Vanmeensel, A.Laptev, O.Van der Biest, J.Vleugels, *Journal of the European Ceramic Society*, **27(2–3)**, 979–985, (2007). doi: https://doi.org/10.1016/j.jeurceramsoc.2006.04.142.
13. V.O.Chyshkala, S.V.Lytovchenko, V.P.Nerubatskyi, R.V.Vovk, E.S.Gevorkyan, O.M.Morozova, *Functional Materials*, **29(1)**, 30–38 (2022). doi: https://doi.org/10.15407/fm29.01.30.
14. E.Hevorkian, R.Michalczewski, M.Rucki, D.Sofronov, E.Osuch-Słomka, V.Nerubatskyi, Z.Krzysiak, J.N.Latosińska, *Ceramics International*, **50(19A)**, 35226–35235 (2024). doi: https://doi.org/10.1016/j.ceramint.2024.06.331.
15. B.Basu, J.Vleugels, O.Van der Biest, *Materials Science and Engineering: A*, **380(1–2)**, 215–221 (2004). doi: https://doi.org/10.1016/j.msea.2004.03.065.
16. E.Gevorkyan, V.Nerubatskyi, V.Chyshkala, O.Morozova, *Eastern-European Journal of Enterprise Technologies*, **5(12(113))**, **6**–**19** **(2021).** doi: https://doi.org/10.15587/1729-4061.2021.242503.
17. E.S.Gevorkyan, D.S.Sofronov, V.P.Nerubatskyi, V.O.Chyshkala, O.M.Morozova, O.M.Lebedynskyi, P.V.Mateychenko, *Journal of Superhard Materials*, **45(1)**, 31–45 (2023). doi: https://doi.org/10.3103/S1063457623010057.
18. H.Y.Ryu, H.H.Nersisyan, J.H.Lee, *International Journal of Refractory Metals and Hard Materials*, **30(1)**, 133–138 (2012). doi: https://doi.org/10.1016/j.ijrmhm.2011.07.015.
19. G.Anné, S.Put, K.Vanmeensel, D.Jiang, J.Vleugels, O.Van der Biest, *Journal of the European Ceramic Society*, **25(1)**, 55–63 (2005). doi: https://doi.org/10.1016/j.jeurceramsoc.2004.01.015.
20. Z.Krzysiak, E.Gevorkyan, V.Nerubatskyi, M.Rucki, V.Chyshkala, J.Caban, T.Mazur, *Materials*, **15(17)**, 6073 (2022). doi: https://doi.org/10.3390/ma15176073.
21. V.P.Nerubatskyi, R.V.Vovk, E.S.Gevorkyan, D.A.Hordiienko, Z.F.Nazyrov, H.L.Komarova, *Low Temperature Physics*, **49(11)**, **1277**–1282 (2023**).** doi: https://doi.org/10.1063/10.0021374**.**
22. M.Mulukutla, A.Singh, S.P.Harimkar, *JOM*, **62**, 65–71 (2010). doi: https://doi.org/10.1007/s11837-010-0090-y.
23. D.V.Dudina, A.K.Mukherjee, *Journal of Nanomaterials*, **2013**, 625218 (2013). doi: https://doi.org/10.1155/2013/625218.
24. Z.A.Munir, *Journal of Materials Synthesis and Processing*, **8**, 189–196 (2000). doi: https://doi.org/10.1023/A:1011312126285.
25. E.S.Hevorkian, V.P.Nerubaskyi, V.O.Chyshkala, S.V.Lytovchenko, M.M.Prokopiv, W.Samociuk, V.A.Mechnik, *Journal of Superhard Materials*, **46(5)**, 364–375 (2024). doi: https://doi.org/10.3103/S1063457624050046.
26. M.Vanlandingham, *Journal of research of the National Institute of Standards and Technology*, **108(4)**, 249–265 (2003). doi: https://doi.org/10.6028/jres.108.024.
27. A.G.Mamalis, E.S.Hevorkian, V.P.Nerybatskyi, M.Rucki, Z.Krzysiak, O.M.Morozova, *Nanotechnology Perceptions*, **19(3)**, **26**–46 (2023**).** doi: https://doi.org/10.56801/nano-ntp.v19i3.325.
28. B.T.Ratov, E.Hevorkian, V.A.Mechnik, N.A.Bondarenko, V.M.Kolodnitskyi, T.O.Prikhna, V.E.Moshchil, V.P.Nerubaskyi, A.B.Kalzhanova, R.U.Bayamirova, A.R.Togasheva, M.D.Sarbopeeva, *Journal of Superhard Materials*, **46(3)**, 175–186 (2024). doi: https://doi.org/10.3103/S1063457624030079.

29. V.P.Nerubatskyi, R.V.Vovk, M.Gzik-Szumiata, E.S.Gevorkyan, *Low Temperature Physics*, **49(4)**, 540–546 (2023). doi: https://doi.org/10.1063/10.0017596.
30. B.T.Ratov, V.A.Mechnik, N.A.Bondarenko, V.M.Kolodnitskyi, E.S.Gevorkyan, V.P.Nerubaskyi, A.G.Gusmanova, B.V.Fedorov, N.A.Kaldibaev, M.T.Arshidinova, V.G.Kulych, *Journal of Superhard Materials*, **45(5)**, 348–359 (2023). doi: https://doi.org/10.3103/S1063457623050088.
31. R.Chaim, M.Hefetz, *Journal of Materials Research*, **13**, 1875–1880 (1998). doi: https://doi.org/10.1557/JMR.1998.0266.
32. E.Tiferet, G.Kimmel, G.Danieli, D.Mogilyanski, O.Yeheskel, *Journal of the European Ceramic Society*, **33(10)**, 1947–1954 (2013). doi: https://doi.org/10.1016/j.jeurceramsoc.2013.03.003.
33. A.B.Nagaram, G.Maistro, E.Adolfsson, Y.Cao, E.Hryha, L.Nyborg, *Metals*, **14(8)**, 914 (2024). doi: https://doi.org/10.3390/met14080914.
34. D.-J.Chen, M.J.Mayo, *Nanostructured Materials*, **2(5)**, 469–478 (1993). doi: https://doi.org/10.1016/0965-9773(93)90164-7.
35. M.Tokita, *Ceramics*, **4(2)**, 160–198 (2021). doi: https://doi.org/10.3390/ceramics4020014.
36. J.R.Groza, *Powder Metallurgy*, **7(2)**, 583–589 (1998).
37. F.Bernard, S.Gallet, N.Spinassou, S.Paris, E.Gaffet, J.N.Woolman, Z.A.Munir, *Science of Sintering*, **36(3)**, 155–164 (2004). doi: https://doi.org/10.2298/SOS0403155B.
38. T.K.Gupta, F.F.Lange, J.H.Bechtold, *Journal of Materials Science*, **13**, 1464–1470 (1978). doi: https://doi.org/10.1007/BF00553200.
39. R.Orrù, R.Licheri, A.M.Locci, A.Cincotti, G.Cao, *Materials Science and Engineering: R: Reports*, **63(4–6)**, 127–287 (2009). doi: https://doi.org/10.1016/j.mser.2008.09.003.
40. G.S.A.M.Theunissen, A.J.A.Winnubst, A.J.Burggraaf, *Journal of the European Ceramic Society*, **11(4)**, 315–324 (1993). doi: https://doi.org/10.1016/0955-2219(93)90031-L.
41. P.Duran, M.Villegas, F.Capel, J.F.Fernandez, C.Moure, *Journal of Materials Science*, **32**, 4507–4512 (1997). doi: https://doi.org/10.1023/A:1018613032145.
42. V.P.Nerubatskyi, E.S.Hevorkian, R.V.Vovk, Z.Krzysiak, H.L.Komarova, *Low Temperature Physics*, **50(7)**, 558–568 (2024). doi: https://doi.org/10.1063/10.0026282.
43. E.D.Whitney, *Journal of the American Ceramic Society*, **45(12)**, 612–613 (1962). doi: https://doi.org/10.1111/j.1151-2916.1962.tb11072.x.
44. K.R.Venkatachari, D.Huang, S.P.Ostrander, W.A.Schulze, G.C.Stangle, *Journal of Materials Research*, **10**, 756–761 (1995). doi: https://doi.org/10.1557/JMR.1995.0756.
45. D.T.Livey, P.Murray, *Journal of the American Ceramic Society*, **39(11)**, 363–372 (1956). doi: https://doi.org/10.1111/j.1151-2916.1956.tb15606.x.